https://doi.org/10.5194/egusphere-2026-4502
Preprint. Discussion started: 4 August 2026

Exploring iron processes in the California Current System through a regional dataset of dissolved iron and organic ligands measurements

Anh Le-Duy Pham[1], Alexis Floback[2,5], Natalya Evans[2,6], Claire Till[3], Ralph Till[3], James Moffett[2], Katherine Barbeau[4], and Daniele Bianchi[1]

[1]Department of Atmospheric and Oceanic Sciences, University of California, Los Angeles, USA
[2]Department of Oceanography, University of Southern California, USA
[3]Moss Landing Marine Laboratories, USA
[4]Scripps Institution of Oceanography, University of California San Diego, USA
[5]Now at: Department of Oceanography, University of Hawai'i at Mānoa, Honolulu, HI, USA
[6]Now at: Department of Oceanography, Dalhousie University, Canada

Correspondence: Anh Le-Duy Pham (anhlpham78@ucla.edu)

Abstract. The micronutrient iron (Fe) regulates productivity across vast regions of the ocean. Along continental margins, dissolved Fe (dFe) concentrations reflect interactions between external sources and internal cycling. Benthic and riverine inputs, together with stabilization by organic ligands, counterbalance biological uptake, scavenging, and precipitation. However, the balance among these processes remains poorly constrained, particularly with respect to the roles of ligands and authigenic Fe precipitation. Here, we compile 3,990 dFe measurements from 29 studies (1987–2024) and 473 measurements of different ligand classes from 7 studies along the U.S. West Coast (USWC), a mostly Fe-limited yet highly productive upwelling system. Most dFe measurements were collected within the upper 50 m, primarily along the central USWC and during summer. dFe concentrations exhibit a strong cross-shore gradient, declining from as much as ∼10 nM near the coast to ∼0.1 nM at 100 km offshore. This pattern is consistent with riverine and benthic inputs nearshore and rapid scavenging and precipitation along the shelf-to-basin pathway. Seasonal variability differs regionally: concentrations are higher in the northern USWC during summer, consistent with upwelling, while higher concentrations in the central and southern regions during winter likely reflect riverine inputs and/or enhanced vertical mixing. Concurrent Fe and ligand measurements are strongly correlated, suggesting a central role for ligands in stabilizing dFe. Positive correlations between dFe and macronutrients highlight the importance of biological uptake and remineralization, whereas negative correlations with oxygen indicate enhanced benthic fluxes under hypoxic conditions. Despite the value of the dataset's coast-wide coverage, gaps in spatial and temporal sampling, along with methodological differences among studies, limit a comprehensive understanding of Fe variability and underlying processes. Improved intercalibration and high-quality measurements of Fe speciation and riverine inputs are needed to better constrain particulate Fe dynamics and coastal dFe enrichment. In addition, sustained long-term time series are essential to resolve the full seasonal cycle of Fe in this highly dynamic region.

https://doi.org/10.5194/egusphere-2026-4502
Preprint. Discussion started: 4 August 2026

1 Introduction

The trace metal iron (Fe) is an essential micronutrient that limits primary production over approximately one-third of the world's surface ocean Tagliabue et al. (2017). The cycling of oceanic Fe is more complex than that of macronutrients due to interactions among multiple external sources and rapid internal cycling processes. Along continental margins, this complexity is further amplified by vigorous circulation Pham et al. (2024), high biological activity Damien et al. (2023b), river runoff Krachler and Krachler (2021); Vieira et al. (2020), and benthic fluxes Elrod et al. (2004); Johnson et al. (1999); Homoky et al. (2021), particularly in productive, low-oxygen waters Severmann et al. (2010); Conway and John (2014); Dale et al. (2015); Lam et al. (2020). Even along well-oxygenated margins, sediments can release substantial amounts of Fe in lithogenic and colloidal forms Homoky et al. (2021), accounting for a significant fraction of the observed Fe inventory Tagliabue et al. (2017, 2023).

Benthic dissolved Fe (dFe) can be transported to the surface via upwelling and vertical mixing Tagliabue et al. (2014) and carried offshore by a range of physical processes Siedlecki et al. (2012); Pham et al. (2024); Lam and Bishop (2008), thereby supplying Fe to remote open-ocean regions. Along the shelf-to-basin transport pathway, dFe may be removed through scavenging, precipitation, and aggregation Tagliabue et al. (2017), particularly where concentrations of dissolved, particulate, and colloidal forms are high Floback et al. (2026); Homoky et al. (2021); Tagliabue et al. (2023); Sofen et al. (2023). Organic ligands, originating from both external sources and in situ microbial production Moffett and Boiteau (2024), can complex with dFe and protect it from these removal processes Buck et al. (2010); Rue and Bruland (1995).

The California Current System (CCS), extending from southern British Columbia to Baja California and encompassing the United States West Coast (USWC), exhibits strong spatial and temporal variability in Fe availability. While portions of the CCS experience Fe limitation, particularly offshore, coastal upwelling regions support highly productive ecosystems, rich biodiversity, and valuable fisheries Till et al. (2019); Evans et al. (2020); McClatchie (2016); Checkley and Barth (2009); Biller and Bruland (2013). Processes along the western margin of North America can supply dFe to severely Fe-limited offshore regions, thereby enhancing productivity across the vast northeastern Pacific Ocean Pham et al. (2024). Given the central role of Fe in the CCS, regional measurements of dFe and ligands have increased substantially in recent decades Boiteau et al. (2019); King and Barbeau (2011); Bundy et al. (2014, 2015, 2016); Till et al. (2019).

In parallel, ocean biogeochemical models have been used to advance understanding of the Fe cycle in the region Siedlecki et al. (2012); Pham et al. (2024); Robinson et al. (2022); Fiechter and Moore (2012); Deutsch et al. (2021). These studies indicate that the Fe cycle in the CCS is shaped by high dissolved and particulate Fe fluxes from low-oxygen sediments Evans et al. (2024); Robinson et al. (2022); Floback et al. (2026), complex and seasonally variable ocean circulation Siedlecki et al. (2012); Damien et al. (2023a, b), and interactions among multiple Fe phases and organic ligands Boiteau et al. (2019); Moffett and Boiteau (2024); Evans et al. (2024); Floback et al. (2026).

Despite these advances, a comprehensive synthesis of Fe measurements along the USWC is still lacking. The only major compilation of dFe measurements is global in scope and consists primarily of open-ocean observations Tagliabue et al. (2012), while regional nutrient compilations for the USWC have yet to incorporate Fe Olsen et al. (2019). A regional synthesis would

https://doi.org/10.5194/egusphere-2026-4502
Preprint. Discussion started: 4 August 2026

help assess current understanding of coastal Fe biogeochemistry, identify relationships between Fe and other variables, and provide a framework for testing hypotheses. For example, the global ocean model by Tagliabue et al. (2023) suggests that authigenic particulate Fe precipitation and colloidal aggregation dominate Fe cycling along the USWC, whereas other studies emphasize the roles of remineralization and riverine inputs in supplying dFe and ligands Buck et al. (2007); Wetz et al. (2006); Chase et al. (2007); Wetz et al. (2006); Vieira et al. (2020). Pham and Ito (2018) proposed that remineralization of sinking particles releases both dFe and ligands into the water column, while Wetz et al. (2006), Chase et al. (2007), and Buck et al. (2007) identified river runoff as an important source of both Fe and ligands in the northern CCS. In addition, given the dominant roles of summertime upwelling and winter mixing in controlling nutrient variability along the USWC Damien et al. (2023b); Jacox et al. (2018b), similar processes are expected to play a leading role in regulating the Fe cycle in the CCS.

Beyond Fe sources and internal cycling, a regional synthesis also provides a framework for testing predictions regarding the physical transport of shelf-derived Fe. Using a submesoscale-permitting circulation model, Pham et al. (2024) showed that a significant fraction ($\sim$20%) of benthic Fe escapes removal on the shelf and is exported to the open ocean, largely via a bottom boundary layer (BBL) pathway associated with the frictional interaction of the poleward California Undercurrent with bottom topography. This export is not uniform along the coast but is instead concentrated at a small number of standing-eddy hot-spots, where cross-shelf transport is enhanced by meanders in the Undercurrent. This prediction of spatially concentrated, BBL-dominated export has yet to be evaluated against direct observations, representing a further hypothesis that a regional Fe compilation is well positioned to test.

In this study, we compile dFe and ligand measurements along the USWC to investigate their spatial and temporal variability and to test hypotheses regarding the dominant processes shaping the coastal Fe cycle. Our objectives are to elucidate the mechanisms controlling dFe and ligand distributions along a productive continental margin, identify key knowledge gaps, and inform future observational efforts.

The remainder of the paper is organized as follows: Section 2 describes the data sources and measurement methods; Section 3 examines the spatial and temporal distributions of dFe and evaluates the roles of ligands and other processes; and Section 4 discusses the results, outlines directions for future work, and concludes the paper.

2 Methods

2.1 Data sources and compilation methods

We assembled data from 29 studies conducted between 1987 and 2024 (Table S1), comprising 3,990 measurements of dFe and 473 measurements of different ligand classes along the USWC. The compilation draws on regional programs such as CalCOFI, CCE-LTER, and MBARI, as well as individual research efforts. A complete list of data sources is provided in Table S1. Of the 29 studies, only 7 include ligand measurements Boiteau et al. (2019); Bundy et al. (2014, 2015, 2016).

In Fe studies, "truly dissolved Fe" is typically defined as Fe that passes through filters with pore sizes of 0.20, 0.40, or 0.45 μm, whereas "total dissolvable Fe" refers to the sum of truly dissolved Fe and the fraction of the particulate Fe pool that dissolves in acid solutions with pH < 1.7. Of the 29 studies included in this compilation, 24 reported truly dissolved Fe

https://doi.org/10.5194/egusphere-2026-4502
Preprint. Discussion started: 4 August 2026

concentrations, whereas 5 reported total dissolvable Fe Fitzwater et al. (2003); Johnson et al. (2003, 2001); Chase et al. (2005); Elrod et al. (2004). For this compilation, we adopt the definitions used in the original studies and report both truly dissolved Fe and total dissolvable Fe under the umbrella term "dFe" throughout the main text, while acknowledging that filter pore sizes, sampling approaches, and sample treatment methods vary among studies. Separate analyses of the truly dissolved Fe and total dissolvable Fe datasets are provided in the Supplementary Material.

Ligand measurements in our compilation were primarily conducted using electrochemical methods, specifically Competitive Ligand Exchange–Adsorptive Cathodic Stripping Voltammetry (CLE-ACSV), applied either with multiple analytical windows Bundy et al. (2014, 2015, 2016) or with a single analytical window Buck et al. (2007); Hogle et al. (2018); King et al. (2012). In this approach, a competing ligand of known concentration and binding strength is added to seawater samples, and the partitioning of the metal between the added and ambient ligands is measured electrochemically by adsorption onto a dropping mercury electrode Gledhill and Buck (2012); Moffett and Boiteau (2024). By coupling these competitive ligand experiments with titrations of added metals, the conditional stability constant (K) and ligand concentration (L) can be determined Gledhill and Buck (2012); Moffett and Boiteau (2024). Ligands are operationally classified into discrete classes based on their binding strengths, with the strongest ligands (L_1, $\log K^{\mathrm{cond}}_{\mathrm{FeL,Fe'}} \geq 12.0$) found at elevated concentrations in highly productive, Fe-depleted waters Gledhill and Buck (2012); Moffett and Boiteau (2024), followed by L_2 ($11.0 \leq \log K^{\mathrm{cond}}_{\mathrm{FeL,Fe'}} < 12.0$), L_3 ($10.0 \leq \log K^{\mathrm{cond}}_{\mathrm{FeL,Fe'}} < 11.0$), and L_4 ($\log K^{\mathrm{cond}}_{\mathrm{FeL,Fe'}} < 10.0$) Bundy et al. (2015); Gledhill and Buck (2012). This method assumes prior knowledge of ligand classes and equilibrium conditions, and requires highly sensitive instrumentation and trace-metal-clean sampling techniques Gledhill and Buck (2012); Moffett and Boiteau (2024). Importantly, while CLE-ACSV provides robust bulk measurements of ligand concentration and binding strength across the whole sample, it cannot provide information on the chemical identity, biological source, or bioavailability of the metal–ligand complexes Moffett and Boiteau (2024).

Alternatively, one study Boiteau et al. (2019) employed liquid chromatography with inductively coupled plasma mass spectrometry and electrospray ionization mass spectrometry (LC-ICPMS-ESIMS). In this approach, metal–organic ligand complexes are first concentrated from seawater using solid-phase extraction, then separated chromatographically, with the eluent simultaneously detected by ICPMS for quantification of metal-bound ligands and by ESIMS for molecular identification Moffett and Boiteau (2024). This method can identify specific individual ligand molecules, such as siderophores (e.g., ferrioxamine B, amphibactins), and reveal how their composition and concentration vary across oceanographic regimes Boiteau et al. (2019); Moffett and Boiteau (2024). However, LC-ICPMS-ESIMS captures only a fraction of the total ligand pool: discrete, chromatographically resolved compounds represent a small portion of the total metals isolated, while the remainder appear as a chromatographically unresolved complex mixture of ligands that cannot be fully separated Moffett and Boiteau (2024). In short, CLE-ACSV quantifies the bulk thermodynamic ligand pool, while LC-ICPMS-ESIMS identifies the molecular nature of a subset of those ligands Moffett and Boiteau (2024).

In our compilation, we report ligand concentrations across different classes defined by their binding strength with Fe or by their chemical structure (L_1, L_2, L_3, L_4, and siderophores, which have more or less same binding strength as L_1). Despite differences in sampling and measurement approaches, we found generally good agreement among the data sources, suggesting

https://doi.org/10.5194/egusphere-2026-4502
Preprint. Discussion started: 4 August 2026

that the compilation provides a reliable representation of dFe and ligand distributions along the USWC. We also acknowledge that residual differences in sampling and analytical methods may introduce biases in the interpretation of the aggregated dataset. To mitigate this, we documented the sampling procedures and analytical treatments used in the original studies whenever possible (see Table S1).

2.2 Co-location with hydrographic observations

To investigate the relationships among dFe, ligands, and hydrographic properties—including temperature, salinity, nutrients, oxygen (O_2), and chlorophyll-*a*—we also incorporated data from a range of regional programs (CalCOFI, CCE-LTER), local surveys, time-series stations, and individual research cruises (see Table S2).

Because these studies did not measure the same parameters, and sampling was not always concurrent or co-located with the Fe and ligand measurements, we mapped the Fe and hydrographic datasets onto a common grid. We used a regular grid with a horizontal resolution of 0.25° and 32 unequally spaced vertical layers, with higher resolution near the surface. All data points within each grid cell were averaged at monthly resolution, irrespective of year, while retaining the number of measurements, as well as the mean, median, and standard deviation of each variable for subsequent statistical analyses.

Finally, we characterized dFe seasonality by constructing monthly climatologies for regions with sufficient observations. To do so, we first aggregated all observations into a single climatological year. From this, we derived three estimates of the seasonal cycle: the geometric mean and the median for each climatological month, and a smooth representation obtained by fitting a cyclical 6-node spline to all observations in the climatological year, following Sandoval-Belmar et al. (2023).

3 Results

3.1 Data distribution

In this compilation, dFe measurements are most abundant in the Southern USWC (28–36°N) (Figure 1 and Figures S1–S2), whereas most ligand measurements are concentrated in the Central USWC (36–40°N) (Figure 2 and Figures S3–S7). Of all dFe measurements, 20% are from the Northern USWC (north of 40°N), 38% from the Central USWC, and 42% from the Southern USWC. Of the 3990 dFe measurements compiled, 1016 are total dissolvable Fe. All total dissolvable Fe measurements are from the Central and Southern USWC, with most originating from the MBARI program Johnson et al. (2001, 2003) (Figure S1). For ligands, 56% of L_1 measurements are from the Southern USWC, whereas 67% of L_2 and 54% of L_3 measurements are from the Central USWC. In contrast, the compilation contains only 16 L_4 measurements and 22 siderophore measurements, most of which are from the Central USWC.

Vertically, most dFe measurements (70%) are from the upper 50 m of the water column, with the remaining 30% collected from subsurface and deep waters (>50 m) (Figure 3). Similarly, more than 50% of the measurements for each ligand class are from the upper ocean (0–50 m; Figure 3).

https://doi.org/10.5194/egusphere-2026-4502
Preprint. Discussion started: 4 August 2026

Across the dataset, dFe concentrations primarily range from 0.1 to 10 nM, with a median of approximately 0.3 nM, whereas ligand concentrations are generally higher than dFe concentrations (Figure 3). Specifically, the strongest ligand class, L_1, has median concentrations of approximately 1–3 nM, while siderophores, despite having binding strengths comparable to those of L_1, have a median concentration of about 0.3 nM, similar to that of dFe. The weaker ligand classes (L_2, L_3, and L_4) all exhibit concentrations that generally exceed those of dFe (Figure 3).

To further analyze the Fe pool, we compare the histograms of truly dissolved Fe with total dissolvable Fe (Figure S8). Both pools exhibit broadly similar central tendencies, with median concentrations of 0.77 nM for truly dissolved Fe and 0.72 nM for total dissolvable Fe, and both distributions peak in the 0.1–1 nM range. However, the two pools differ in their vertical distributions. Whereas truly dissolved Fe measurements are more evenly distributed between the upper ocean and subsurface/deep waters, total dissolvable Fe measurements are overwhelmingly concentrated in the upper 50 m (86%), reflecting the more limited depth coverage of the total dissolvable Fe dataset. Total dissolvable Fe also exhibits a more pronounced high-concentration tail than truly dissolved Fe, with concentrations exceeding 100 nM occurring almost exclusively in near-surface samples (0–50 m). These elevated concentrations likely reflect locally enhanced particulate and colloidal Fe inputs, such as resuspended sediments or terrigenous material, that are retained in the acid digestion but excluded from measurements of the truly dissolved fraction.

3.2 Spatial variability of dFe and ligands

On average, coastal dFe concentrations (within 50 km of the coast, defined relative to the 200 m isobath) are relatively high in surface waters (∼1 nM), increase to a subsurface maximum of up to ∼10 nM at around 100 m, decline to ∼3 nM near 300 m, and then increase again to a deep maximum (>10 nM) near 1000 m (Figure 4). In contrast, offshore dFe concentrations (>50 km from the coast) are lower and more uniform in surface waters (0.2–0.3 nM), increase to approximately 0.5 nM at around 250 m, and remain relatively stable (0.7–1 nM) throughout the deeper water column.

When the truly dissolved and total dissolvable Fe pools are examined separately (Figures S9–S10), they exhibit different vertical distributions. Coastal truly dissolved Fe (Figure S9) shows the same near-surface concentration (∼1.5–1.7 nM) and subsurface maximum (up to ∼9–10 nM at 60–100 m) as the combined profile, but then declines to ∼2–3 nM between 100 and 300 m and increases only modestly to ∼4–6 nM between 500 and 1000 m. These concentrations are well below the >10 nM deep maximum apparent in the combined Fe profile. Offshore truly dissolved Fe remains low and increases gradually with depth, from ∼0.2–0.3 nM near the surface to ∼0.7–0.9 nM at 300–400 m and ∼1–1.5 nM between 500 and 2500 m, without the pronounced subsurface and deep maxima observed in the coastal profile. In contrast, coastal total dissolvable Fe (Figure S10) is both higher in concentration and substantially more variable at depth. Concentrations reach a broad subsurface maximum of approximately 3–20 nM between 40 and 100 m, and several deep samples (300–1000 m) exhibit markedly elevated concentrations ranging from tens to several hundred nM, although these values are based on only 2–4 observations. Offshore total dissolvable Fe is comparatively lower and more uniform throughout the upper few hundred meters (∼0.4–2.5 nM), while the sparse sampling below ∼200 m precludes robust conclusions about its deep distribution. These separate profiles indicate that the apparent deep (>500 m) Fe enrichment in the combined coastal profile is driven primarily by a small number

https://doi.org/10.5194/egusphere-2026-4502
Preprint. Discussion started: 4 August 2026

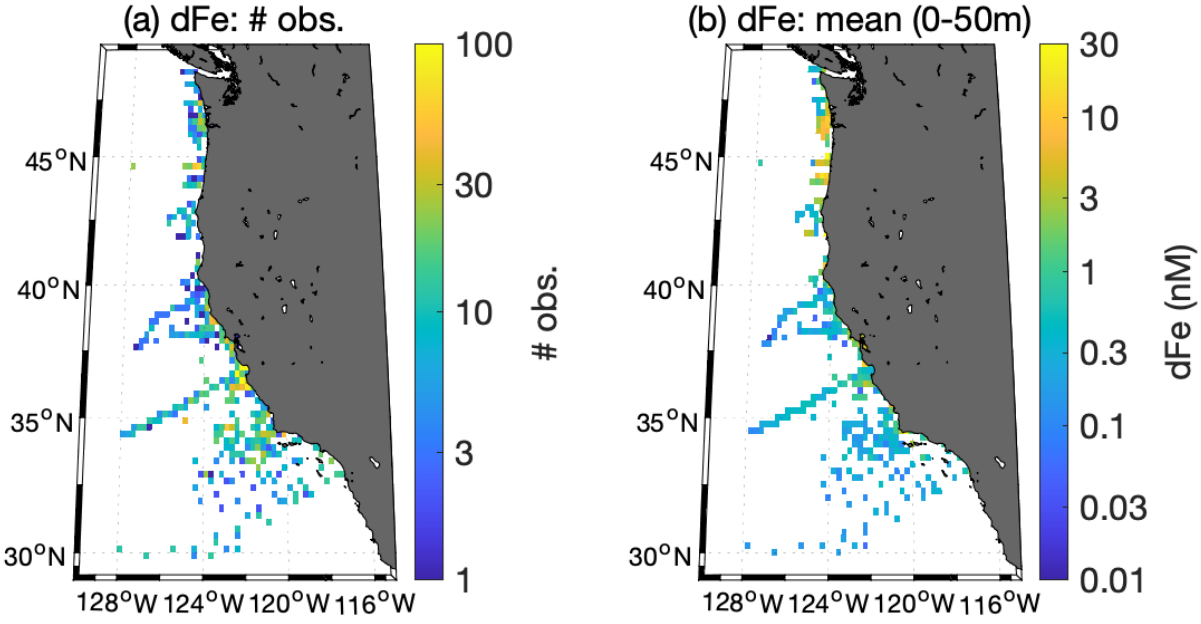

Figure 1. Dissolved iron dataset from the US West Coast. (a) Number of dissolved iron (dFe) measurements for al depth levels within spatial cells of 0.25°x 0.25°horizontal resolution. (b) Mean dFe concentration (nM) in the 0-50 m depth range, averaged over the 0.25°x 0.25°cells shown in (a).

of elevated total dissolvable Fe measurements rather than by the truly dissolved fraction, which remains comparatively low and stable with depth.

Horizontally, surface dFe concentrations (averaged over the upper 50 m) are low (∼0.1 nM) in the open ocean but increase to as much as ∼10 nM in coastal areas of the Southern USWC and ∼30 nM along the northern coast (Figure 1b; Figure 5), forming pronounced cross-shore and meridional gradients. The steepest cross-shore decline occurs within the first 100 km of the coastline (Figure 5b). More generally, dFe concentrations are elevated nearshore throughout the water column, with maxima occurring in surface waters and near the seafloor (Figures 4 and 5), consistent with continental margin sources such as riverine inputs and shallow benthic Fe fluxes Chase et al. (2007); Severmann et al. (2010); Robinson et al. (2022). Offshore, dFe decreases more gradually in the upper 100 m (from ∼1 nM to ∼0.1 nM), with even weaker cross-shore gradients in deeper waters (Figure 5).

https://doi.org/10.5194/egusphere-2026-4502
Preprint. Discussion started: 4 August 2026

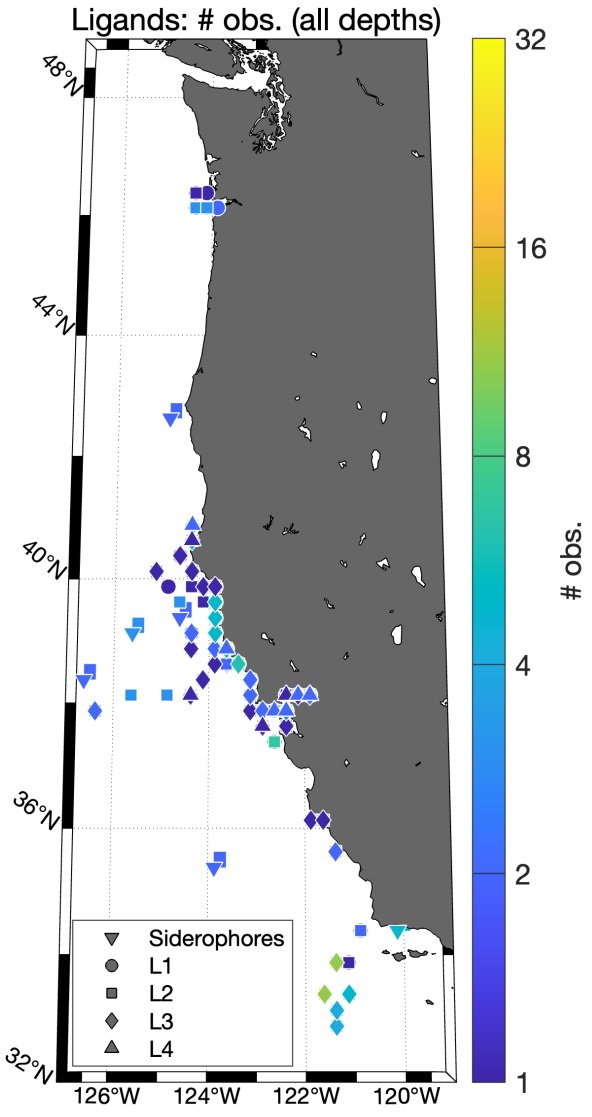

Figure 2. Ligand dataset from the US West Coast. Number of ligand measurements for all depth levels within spatial cells of 0.25°x 0.25°horizontal resolution. Different symbols represent different types of ligands (Siderophores, L1, L2, L3, and L4 - see the legend and section 2)

https://doi.org/10.5194/egusphere-2026-4502
Preprint. Discussion started: 4 August 2026

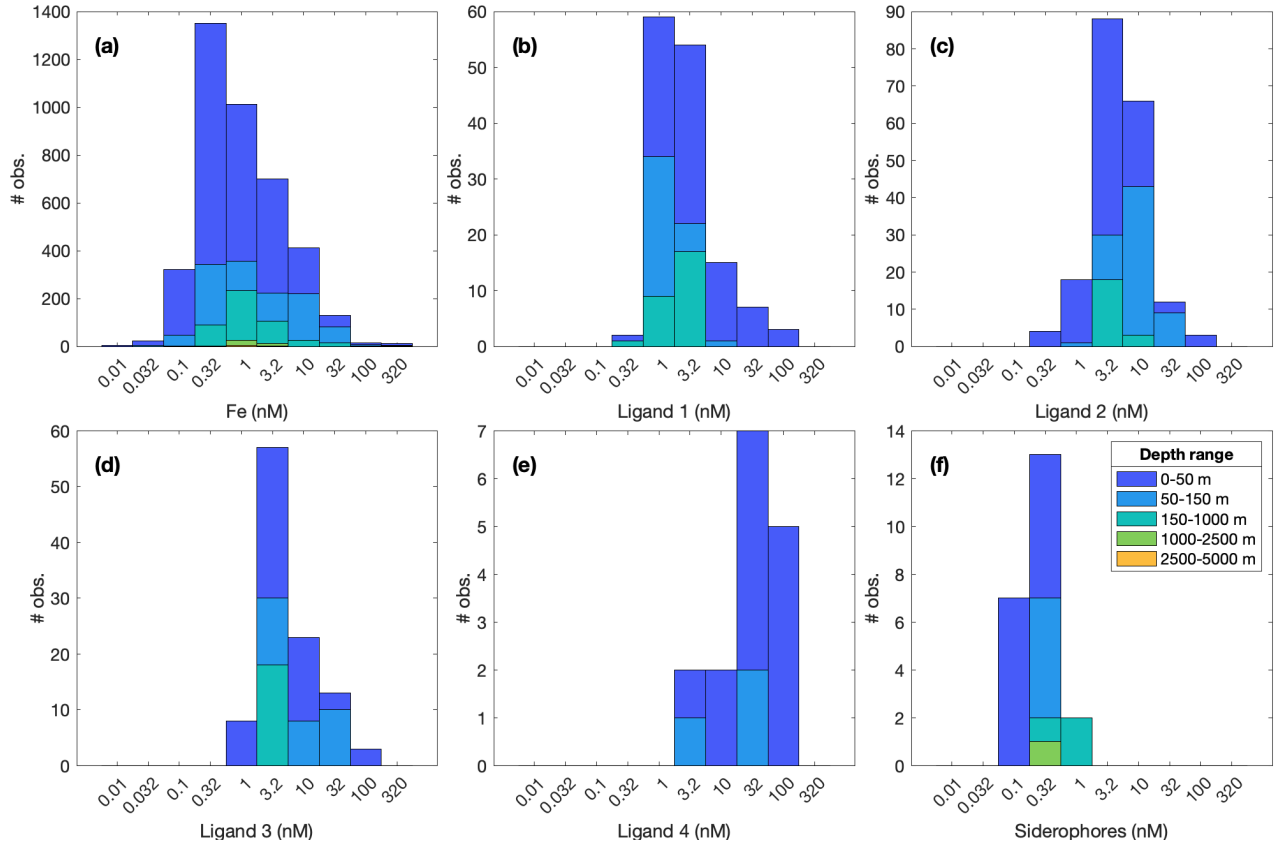

Figure 3. Histograms showing the number of measurements as a function of concentrations for (a) dissolved iron (dFe, nM) and for different ligand types(nM): (b) L1, (c) L2, (d) L3, (e) L4, (f) Siderophores, along the US West Coast, based on the data compilation. Colors show different depth ranges.

When the truly dissolved and total dissolvable Fe pools are examined separately, the truly dissolved Fe cross-shore sections (Figure S11) reproduce the overall structure of the combined Fe dataset. Elevated concentrations remain confined to the nearshore surface and bottom boundary layer, with a comparatively gradual, nearly linear decline across the upper 100 m moving offshore. This indicates that the nearshore surface and bottom-intensified Fe enrichment is a robust characteristic of the truly dissolved fraction itself. In contrast, the total dissolvable Fe sections (Figure S12) exhibit a much more spatially confined cross-shore signal. The highest concentrations (approaching the upper limit of the color scale, ∼32 nM) are restricted almost entirely to shallow shelf waters (<500 m bottom depth) within approximately 10–50 km of the coast. Concentrations then decrease rapidly to ∼0.1–0.3 nM within roughly 100–200 km offshore. Sampling of total dissolvable Fe is also considerably sparser at depth than that of truly dissolved Fe, with only a handful of profiles extending below 500 m. These deeper observations, located at intermediate distances (∼100–300 km) from the coast, show comparatively low concentrations (∼1–3

https://doi.org/10.5194/egusphere-2026-4502
Preprint. Discussion started: 4 August 2026

nM) rather than an elevated nearshore signal, and there is essentially no coverage beyond ∼300 km offshore or below ∼2000 m depth.

Surface ligand concentrations are generally higher than dFe concentrations (Figures S3–S7). For example, concentrations of L_2, L_3, and L_4 reach up to 30 nM (e.g., near 33°N and 38°N) and remain consistently above 1 nM from the coast to the open ocean for all ligand classes except siderophores (Figures S3–S7). On average, concentrations of ligands (L_1, L_2, L_3, and L_4) range between 1 and 10 nM in surface waters, where variability is high. Concentrations increase in the subsurface, with pronounced nearshore maxima occurring at approximately 50 m for L_1 and around 100 m for L_2, L_3, and L_4. These subsurface maxima are likely associated with the seafloor over the upper continental shelf and are accompanied by substantial spatial variability (Figure S13). Farther offshore (>100 km), concentrations are more stable, increasing gradually with depth from about 3 nM near the surface to approximately 10 nM at 1000 m (Figure S13). Notably, ligand measurements reported by Boiteau et al. (2019), based on the LC-ICPMS-ESIMS method (see Section 2.1), are consistently lower than those obtained using the CLE-ACSV method—by up to an order of magnitude—and exhibit lower variability (Figure S13).

3.3 Seasonality dFe along the US West Coast

We analyzed the seasonality of dFe in the euphotic zone (0–30 m) across different regions of the USWC: Northern (>40°N), Central (36–40°N), Southern (28–36°N), and offshore regions (the latter defined based on the 200 m isobath; Figure 6). In the Northern region, data are primarily available from April to August and largely originate from recent studies (Evans et al. (2024); Floback et al. (2026)). In the Central region, July has the highest number of measurements, although a substantial number of observations span the entire year, mostly reflecting the extensive time series of Johnson et al. (2001); Elrod et al. (2008), which account for approximately 32% of the surface observations. In the Southern region, the CalCOFI and CCE-LTER programs provide year-round coverage King and Barbeau (2011). Offshore regions also include year-round data, with most samples collected in March and July.

In the Northern region, where data are sparse, we detect a dFe peak in June (∼7 nM), followed by a rapid decline thereafter. In the Central region, dFe peaks in February (∼2 nM) and then declines to a minimum in June (∼0.2 nM), although variability is high. In the Southern region, where data coverage is densest, dFe peaks in winter (∼2 nM) and declines through spring and summer to a minimum in fall. The offshore region exhibits weaker seasonal variability, with concentrations ranging from a maximum of 0.4 nM in March to a minimum of 0.2 nM in May. A comparable analysis was not possible for ligands due to data sparsity.

3.4 Relationships between Fe and ligands and environmental variables

We examine the relationships among the distributions of dFe, ligands, and other hydrographic variables along the USWC (Figures 7, 8, 9, and 10). As described in the Methods, hydrographic samples were not collected synchronously with Fe and ligand measurements. Instead, to generate a consistent dataset, we co-located all observations (Fe, ligands, and hydrographic variables) by mapping them onto a regular grid at monthly resolution, irrespective of year, thereby producing climatological fields (see Section 2.2).

https://doi.org/10.5194/egusphere-2026-4502
Preprint. Discussion started: 4 August 2026

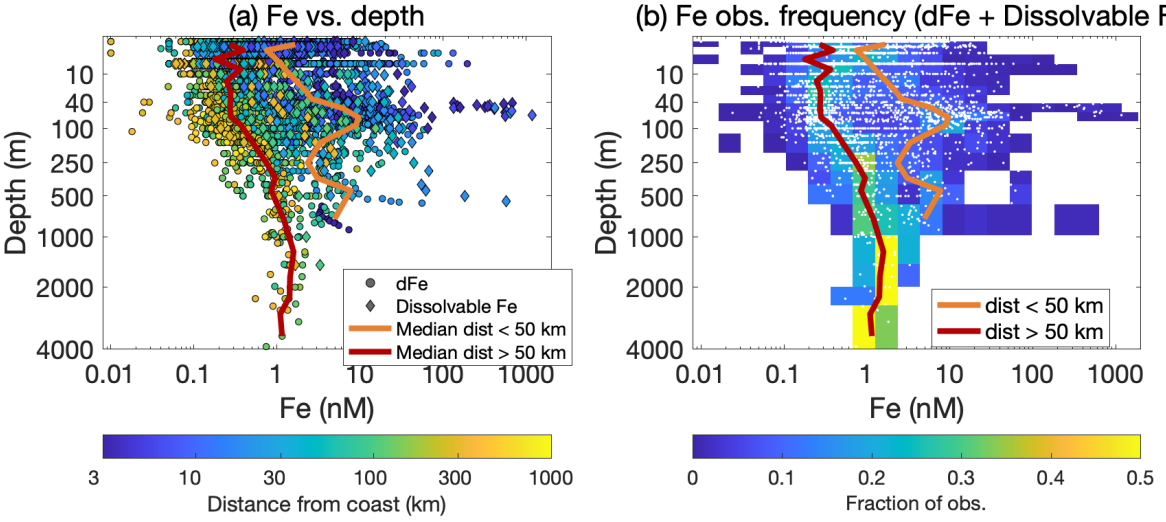

Figure 4. (a) Vertical profile of dissolved iron (dFe, nM) measurements along the US West Coast. Each dot represents a measurement, with colors showing the distance from shore (km). Circles represent truly dissolved Fe, while diamonds represent dissolvable Fe. Solid orange and red lines show the median dFe for nearshore ($<$ 50 km) and offshore ($>$ 50 km) measurements, respectively. (b) Density distribution of dFe samples as a function of depth. Background colors show the probability distribution of dFe measurements at each depth, calculated as the fraction of measurements with a given concentration in each depth layer. White dots show individual measurements; solid orange and red lines the median dFe for nearshore ($<$ 50 km) and offshore ($>$ 50 km) measurements, respectively.

Synchronous measurements of dFe and ligands Boiteau et al. (2019); Bundy et al. (2014, 2015, 2016); Buck et al. (2007); Hogle et al. (2018); King et al. (2012) show strong and statistically significant correlations (Pearson's linear correlation coefficient R = 0.96, 0.92, 0.98, 0.97, and 0.75 for dFe versus L_1, siderophores, L_2, L_3, and L_4, respectively), with concentrations increasing together across both low and high ranges, as evident on both linear (Figure 7a) and logarithmic scales (Figure 7b). On a logarithmic scale (Figure 7b), distinct relationships between dFe and different ligand types emerge. Siderophore concentrations are approximately one order of magnitude lower than those of other ligand classes and are generally lower than dFe concentrations. Strong ligands L_1 and L_2 cluster around the 1:1 line, indicating that their concentrations are broadly comparable to dFe concentrations at the same locations and suggesting a tight coupling between dFe and iron-complexation capacity. In contrast, concentrations of the weaker ligands L_3 and L_4 exhibit greater variability and generally exceed dFe concentrations, implying an excess ligand pool relative to dFe.

dFe exhibits significant positive correlations with PO_4^{3-}, NO_3^-, and $Si(OH)_4$ (R = 0.4–0.5), and a weaker positive correlation with NO_2-(R = 0.27) (Figure 8). These relationships are also evident in the scatter plots (Figures 9e,f), where dFe concentrations increase from ∼0.1 nM in nutrient-depleted surface waters to around 10 nM and locally up to 100 nM in deeper, nutrient-rich waters. In contrast, ligand concentrations remain relatively stable across nutrient gradients (Figures 10e,f). Among

https://doi.org/10.5194/egusphere-2026-4502
Preprint. Discussion started: 4 August 2026

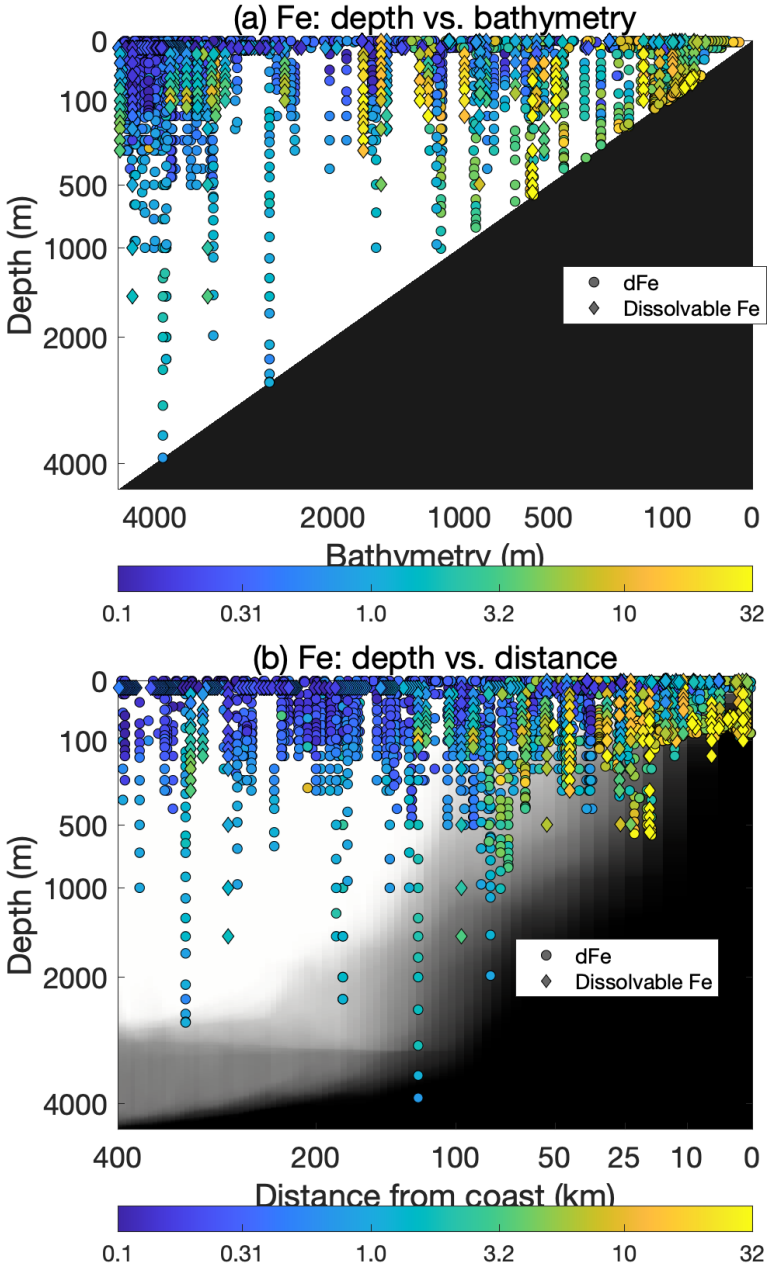

Figure 5. Dissolved iron (dFe, nM) distribution along the US West Coast continental margin as a function of (a) seafloor depth (m) and (b) distance from shore (km). Seafloor depth is derived from the ETOPO bathymetry database at 15" resolution. In (a), black shading indicates locations below the seafloor. In (b), grayscale shading shows a histogram of bottom depths, calculated as the proportion of water column vs. seafloor at each distance bin, ranging from 100% water column (white) to 100% below seafloor (black). Circles represent truly dissolved Fe, while diamonds represent dissolvable Fe.

https://doi.org/10.5194/egusphere-2026-4502
Preprint. Discussion started: 4 August 2026

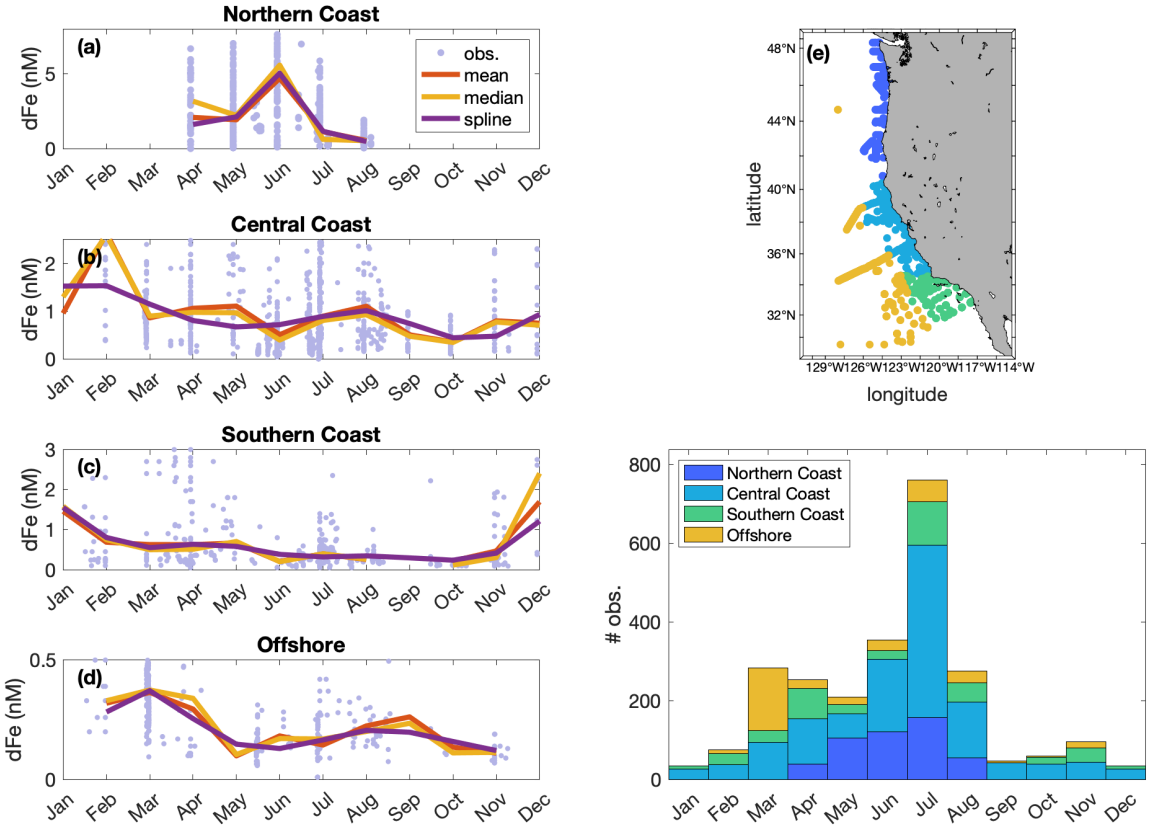

Figure 6. Seasonal variability of surface (0-50 m) dissolved iron (dFe) along the US continental margin. The left panels show the seasonal cycle of dFe concentrations in the (a) the Northern, (b) Central, and (c) Southern US West Coast, and in (d) offshore waters of the USWC. Three approaches are used to estimate the climatological cycle: the geometric mean of monthly data, the geometric median of monthly data, and a 6-node spline fit to the dFe concentrations as a function of day of the year. (e) Location of dFe measurements colored by region (Northern, Central, and Southern Coast, and Offshore waters). (f) Histogram showing the number of dFe measurements for the regions shown in (e).

https://doi.org/10.5194/egusphere-2026-4502
Preprint. Discussion started: 4 August 2026

the ligand classes, L_2 exhibits positive correlations with macronutrients, whereas L_1 shows positive correlations with $Si(OH)_4$ and NO_2-(Figure 8).

The strongest spatial gradients in dFe occur with proximity to the continental margin. dFe exhibits negative correlations with distance from the coast (R = -0.56), distance to the bottom (R = -0.70), and bottom depth (R = -0.65) (Figure 8). Correspondingly, dFe concentrations decrease from ∼10–100 nM in shallow nearshore waters to ∼0.1 nM in offshore waters more than ∼1000 km from the coast and above bottom depths of ∼1000 m (Figures 9a,b). Ligand concentrations show similar offshore declines (Figures 10a,b), although the responses differ among ligand classes. L_1, L_2, and L_3 all exhibit negative correlations with distance from the coast, while L_1 and L_3 also decrease with increasing bottom depth (Figure 8).

dFe is negatively correlated with temperature (R = -0.42; Figure 8), with concentrations decreasing from around 10 nM at 5–10 °C to approximately 0.1 nM at 15–20 °C (Figure 9c). In contrast, ligand concentrations remain relatively stable across the same temperature range (Figure 10c), although L_2 exhibits a weak negative correlation with temperature (Figure 8).

In general, dFe does not exhibit a significant correlation with salinity (Figure 8). Nevertheless, elevated dFe concentrations (∼10 nM) occur under two distinct salinity regimes (Figure S17): in low-salinity (26–27 PSU) near-surface waters and in high-salinity (34–35 PSU) deep waters at depths of around 1000 m. Elevated dFe concentrations in low-salinity surface waters suggest a riverine source of dFe, whereas elevated concentrations in high-salinity deep waters suggest bottom boundary layer sources. Among the ligand classes, only L_1 exhibits a significant relationship with salinity, with elevated concentrations associated with low-salinity waters (Figure 8 and Figure 10).

dFe exhibits a weak negative correlation with O_2 (R = -0.29; Figure 8), although the relationship is not monotonic and likely reflects interactions with other factors, particularly water depth. As shown in Figure 9d, elevated dFe concentrations (∼10 nM) occur at low O_2 concentrations (<10 μM) and tend to increase as O_2 declines in waters between 500 and 1000 m depth. Near the surface (<100 m), where O_2 concentrations are generally high (∼100–300 μM), dFe spans a wide range from less than 0.1 nM to more than 100 nM. Ligand concentrations remain comparatively stable with increasing O_2 (Figure 10d), except for siderophores, which exhibit a strong negative correlation with O_2 (R = -0.86) and a strong positive correlation with pressure (R = 0.70), reaching concentrations of approximately 1 nM under nearly anoxic conditions (Figure 8 and Figure S18).

Overall, dFe exhibits stronger and more consistent relationships with hydrographic variables than the ligands. The pronounced decreases in dFe from the coast to the open ocean, from shallow to deep bottom depths, and from warm to cold waters are consistent with strong continental margin sources and progressive removal during offshore transport. In contrast, most ligand classes remain comparatively stable across environmental gradients, with individual ligand classes exhibiting distinct relationships with specific hydrographic variables, reflecting differences in their sources, production pathways, and persistence in the water column.

To assess whether these relationships differ between the truly dissolved and total dissolvable Fe pools, we repeated the correlation and scatter plot analyses separately (Figures S14–S16). Overall, both pools exhibit similar relationships with hydrographic variables, including negative correlations with distance from the coast, distance to the bottom, bottom depth, temperature, and O_2, and positive correlations with NO_3^-, PO_4^{3-}, and $Si(OH)_4$ (Figure S19). However, the total dissolvable Fe pool generally exhibits slightly stronger correlations with macronutrients (R = 0.49–0.50 versus 0.45–0.56 for truly dissolved Fe),

https://doi.org/10.5194/egusphere-2026-4502
Preprint. Discussion started: 4 August 2026

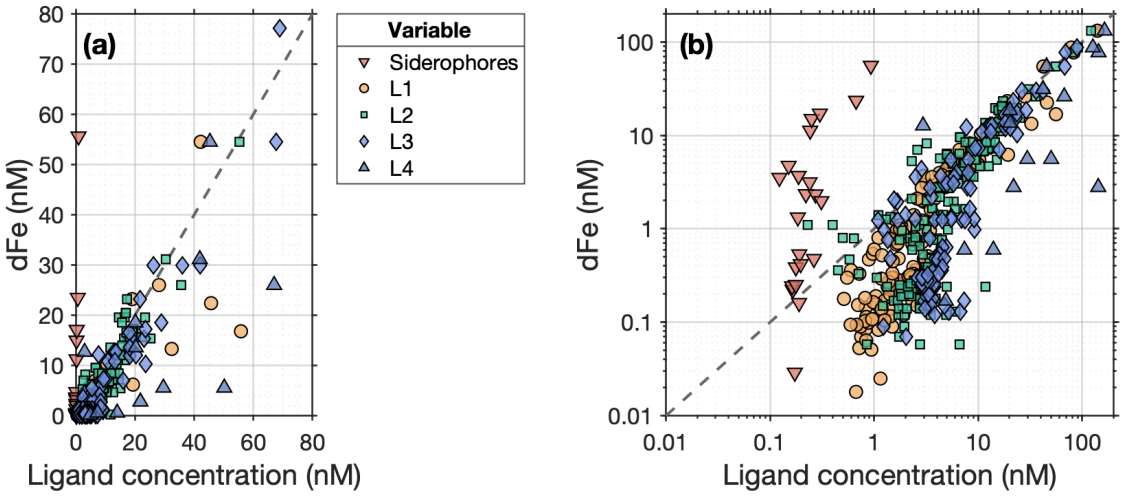

Figure 7. Relationship between dissolved iron (dFe, nM) and ligand (nM) concentrations measured simultaneously along the US West Coast on (a) a linear scale and (b) a logarithmic scale. Colors show the depth of the samples (m). In both panels, the dashed line is the 1:1 line. Different colored symbols represent different types of ligands (Siderophores, L1, L2, L3, and L4 - see the legend and section 2).

pressure (R = 0.42 versus 0.16), salinity (R = 0.46, compared with no significant correlation for truly dissolved Fe), and O_2 (R = -0.39 versus -0.30) (Figure S14).

These differences are also evident in the scatter plots (Figures S15–S16). The truly dissolved Fe pool (Figure S15) reproduces the same broad patterns described for the combined dataset, with concentrations decreasing offshore and with increasing temperature, and increasing with macronutrients and proximity to the seafloor. In contrast, total dissolvable Fe (Figure S16) exhibits substantially greater variability, particularly at high concentrations. Elevated total dissolvable Fe concentrations (>100 nM) occur primarily in shallow, nearshore waters characterized by low temperatures, low O_2, and high macronutrient concentrations, whereas offshore concentrations rapidly decline to values comparable to those of the truly dissolved Fe pool. These results indicate that the major hydrographic controls identified in the combined dataset are robust, while the additional variability in total dissolvable Fe primarily reflects localized particulate and colloidal Fe inputs in shallow coastal environments.

4 Discussion and Conclusion

We compiled measurements of Fe and organic ligands along the USWC from the available literature with several objectives: to identify gaps in our current understanding of the oceanic Fe cycle in the USWC, to evaluate hypotheses regarding the key processes controlling Fe distributions, and to provide a valuable dataset for model validation and future analyses.

A first notable finding is the strong relationship between dFe and all ligand types (R = 0.7–0.9). Concentrations of dFe and ligands increase together, and ligand concentrations are often higher than dFe concentrations, except for siderophores, which represent only a small fraction of the ligand pool Moffett and Boiteau (2024). This result highlights the close coupling

https://doi.org/10.5194/egusphere-2026-4502
Preprint. Discussion started: 4 August 2026

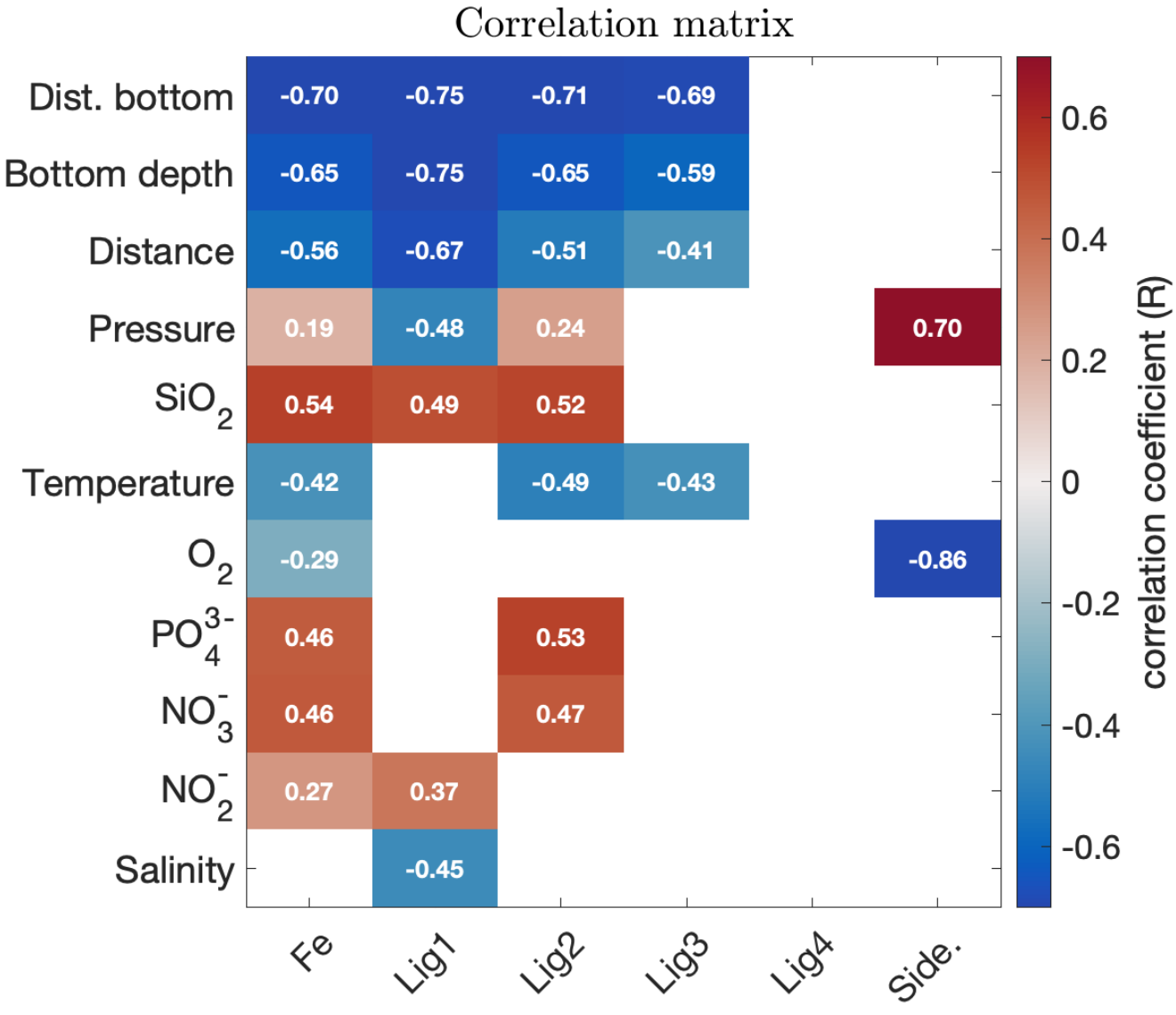

Figure 8. Correlation coefficients between dissolved iron (dFe, nM) and different ligand classes (Lig, nM) concentrations and other co-located environmental variables. Co-location was performed by averaging all variables onto a horizontal grid with a resolution of 0.25°x0.25°(see Figure 1), and does not consider the time of year of the observations. Log-transformations of all variables were taken before calculating the correlations. From top to bottom in the y axis: distance to the bottom, bottom depth, distance from the coast, pressure, silicate ($Si(OH)_4$), temperature, O_2, phosphate (PO_4^{3-}), nitrate (NO_3-), nitrite (NO_2-), and salinity. Only correlations significant at $p<0.01$ are shown.

https://doi.org/10.5194/egusphere-2026-4502
Preprint. Discussion started: 4 August 2026

between dissolved Fe and organic ligands in the CCS, consistent with previous studies Boiteau et al. (2019); Bundy et al. (2014, 2015, 2016); Buck et al. (2007). At the same time, it does not preclude an important role for authigenic particles in regulating the coastal Fe cycle. For example, Tagliabue et al. (2023) proposed that authigenic particles may dominate Fe removal near continental margins through the "colloidal shunt" process. Our compilation, which focuses on dissolved Fe and ligand measurements and does not include particulate Fe observations, cannot directly evaluate the relative importance of these mechanisms. Instead, our results demonstrate that dissolved Fe remains tightly coupled to the ligand pool across a wide range of environmental conditions, emphasizing the need for future studies that simultaneously quantify dissolved Fe, ligand composition, and particulate Fe to better constrain their respective roles in controlling the coastal Fe cycle.

Second, we found strong correlations between the distributions of dFe, macronutrients, and O_2. The positive correlations between dFe and macronutrients highlight the role of biological uptake and remineralization in depleting dFe in the euphotic zone and replenishing it in subsurface waters Pham and Ito (2018); Bruland and Lohan (2003). The negative correlation between dFe and O_2 supports the influence of remineralization processes in the water column and may also reflect sedimentary inputs, as benthic dFe fluxes increase rapidly under low O_2 conditions Severmann et al. (2010); Robinson et al. (2022).

We also identify distinct relationships between different ligand types and macronutrients, as well as other hydrographic variables. Specifically, the strong ligand L_1 shows a negative correlation with salinity, consistent with previous studies Bundy et al. (2014); Buck et al. (2007). Siderophores exhibit a strong negative correlation with O_2, while the moderately weak ligand L_2 shows strong positive correlations with macronutrients. In contrast, the weaker ligand classes L_3 and L_4 do not exhibit significant relationships with macronutrients, O_2, temperature, and salinity. The strong correlations between L_2 and macronutrients, and between siderophores and O_2, support the common assumption in ocean biogeochemical models that ligands are produced during remineralization and via organic matter exudation Pham and Ito (2018); Völker and Tagliabue (2015). In particular, the negative correlation between O_2 and siderophores (the strongest correlation in Figure 8) is consistent with observations in the North Pacific linking siderophore accumulation to heterotrophic respiration in the subsurface "twilight zone" Li et al. (2024). However, the weak correlations of other ligand classes with macronutrients and O_2 suggest that ligand sources and transformations may be partly decoupled from remineralization processes—particularly in coastal regions—and remain incompletely understood. These contrasting behaviors also have important implications for ocean biogeochemical models. Most current models either represent ligands as a single homogeneous pool or assume that all ligand classes share similar production and loss pathways. Our results suggest that this simplification may overlook important differences among ligand classes. In particular, the distinct relationships of L_1, L_2, and siderophores with hydrographic variables indicate that at least some ligand classes respond to different environmental controls and may therefore require separate parameterizations as observations and mechanistic understanding continue to improve.

Previous studies have proposed that ligands can be produced by bacteria under Fe-limited conditions Tortell et al. (1996) and may also have terrestrial origins, entering the ocean via river runoff Vieira et al. (2020). Our compilation reveals a significant negative correlation between the strong ligand L_1 and salinity and distance from the coast, implying a role for riverine and terrestrial sources. Given the limited number of ligand measurements in our dataset, these interpretations remain tentative.

https://doi.org/10.5194/egusphere-2026-4502
Preprint. Discussion started: 4 August 2026

Additional observations in estuarine environments, particularly along the northern USWC, are needed to further evaluate hypotheses regarding ligand sources and production Hassler et al. (2025).

Data in our compilation also show a pronounced decline in dFe concentrations from coastal to open-ocean regions (from from ∼30 nM to ∼0.1 nM). The highest dFe concentrations (up to ∼30 nM) were observed only in localized environments, such as near river mouths and in bottom waters immediately above shelf sediments. This steep gradient, spanning several orders of magnitude across the water column, is unlikely to be explained by biological uptake alone and instead likely reflects rapid dFe removal via particle scavenging along the shelf-to-basin transport pathway Pham et al. (2024); Wong et al. (2022).

Along the Northern coast, particularly high surface dFe concentrations (∼195 nM at 44 °N) may reflect enhanced inputs from river runoff Buck et al. (2007); Wetz et al. (2006); Chase et al. (2007). Previous studies by Chase et al. (2007) and Wetz et al. (2006) suggest that the broad continental shelf of the Northern USWC acts as a capacitor for dFe, accumulating river-derived Fe in winter—when high river discharge and downwelling isolate the shelf from the open ocean—and releasing it during summer upwelling.

However, in our compilation, the correlation between dFe concentrations and salinity—an immediate proxy for river inputs—is weak and not statistically significant across the whole region and year, suggesting some degree of decoupling between riverine input and dFe accumulation in the water column. Additional measurements of dFe in rivers and along the USWC during winter, when runoff intensifies following heavy precipitation, as well as studies of interactions between river-derived material and shallow sediment environments, are needed to test hypotheses regarding the role of riverine Fe supply.

The weak relationship between dFe and salinity is notable given the strong nitrate–salinity relationship documented for this region Gangrade et al. (2025). Rather than indicating an absence of water-mass control on dFe, this weak correlation may instead reflect the superposition of multiple Fe source terms in a basin-wide analysis. To explore this possibility, we restricted the analysis to coastal, off-shelf observations (distance $\leq$ 70 km; bottom depth $>$100 m) (Figures S20–S22). Under these conditions, both Fe pools exhibit a coherent concentration maximum centered within the 25.8–26.5 kg m^{-3} isopycnal band. This density range coincides with the core of the California Undercurrent (CUC) identified by Bograd et al. (2019). The Fe enrichment is also associated with a spiciness signal that is positive in the southern USWC and becomes progressively more negative northward, consistent with the poleward transport of warm, saline, nutrient-rich—and apparently Fe-rich—Pacific Equatorial Water by the CUC beneath the fresher California Current Lynn and Simpson (1987); Zaba et al. (2021). This interpretation is also consistent with the observations of Forsch et al. (2023), who identified elevated dissolved Fe associated with recently upwelled California Undercurrent waters in southern California Current upwelling filaments, suggesting that the CUC serves as an important subsurface source of Fe to the coastal ocean. These observations therefore suggest that dFe is coupled to water-mass properties along isopycnal surfaces and that the CUC represents a subsurface Fe source distinct from the low-salinity, riverine Fe input observed in surface waters. Consequently, elevated dFe concentrations may be associated with either low-salinity river plumes or high-salinity CUC waters, obscuring a simple linear relationship between dFe and salinity when observations from different water masses are considered together. This interpretation remains tentative since station coverage along the CUC core isopycnals is uneven, and the present compilation lacks direct velocity or transport measurements needed to distinguish poleward advection from local remineralization or sedimentary Fe inputs at similar depths. Nevertheless,

https://doi.org/10.5194/egusphere-2026-4502
Preprint. Discussion started: 4 August 2026

these results identify the CUC as a plausible control on coastal dFe distributions and motivate future observations targeting its core isopycnal surfaces.

While the preceding analysis suggests that the CUC may act as a large-scale subsurface transport pathway for Fe, numerical models further predict that this transport is concentrated at a limited number of localized shelf-to-basin export hot-spots. A previous modeling study Pham et al. (2024) identified hot-spots of enhanced shelf-to-basin Fe transport at Heceta Bank (43.95°N), Nehalem Bank (45.95–46.40°N), and the Northern Juan de Fuca Canyon (48.23–48.50°N), with secondary hot-spots near Cape Blanco (43°N) and Grays Canyon (47.04°N), where standing meanders in the California Undercurrent drive export predominantly through the bottom boundary layer (BBL, 175–200 m), accounting for roughly twice the transport of the surface pathway (46% versus 19%). Our compilation, however, cannot test this prediction because BBL-depth (150–250 m) observations near these hot-spots are extremely sparse: only 6 of 63 nearby measurements at Heceta Bank fall within the BBL depth range, while no samples below 91 m are available at Nehalem Bank and no samples deeper than 5 m exist at the Juan de Fuca Canyon site. We therefore recommend that future field campaigns prioritize repeat, depth-resolved BBL sampling at these specific locations, rather than the broader shelf surveys that have historically dominated USWC Fe sampling, to directly test the physical mechanisms predicted to govern shelf-derived Fe export along this margin.

Although the spatial pathways of Fe transport remain poorly constrained, another important uncertainty concerns the chemical form in which Fe is transported. Elevated dFe concentrations are a persistent feature throughout the coastal USWC, but some of the data in our compilation report dissolvable Fe—i.e., particulate Fe that dissolves at pH 1.7 (see Methods)—in addition to truly dissolved Fe. Previous studies Johnson et al. (2001); Elrod et al. (2008); Homoky et al. (2021) suggest that dissolvable Fe forms are abundant along margins due to benthic release and/or river discharge. A recent survey along the Oregon coast Floback et al. (2026) reported remarkably high particulate Fe concentrations in the subsurface ocean (200–500 m), exceeding dFe concentrations by more than an order of magnitude. These elevated particulate Fe concentrations could significantly influence dFe levels through dissolution and desorption, even though the model results by Floback et al. (2026) did not indicate a strong signal of dFe dissolution from particles. Additional measurements targeting different Fe species along the USWC and their interactions—including reversible scavenging—are needed to better constrain the role of particulate Fe.

By analyzing seasonal surface dFe time series (Figure 6, we identify a peak in dFe concentrations in the Northern region in July, coincident with upwelling (as indicated by the Coastal Transport Upwelling Index, CUTI; Figure S19; Jacox et al. (2018a)). However, with few observations in winter, it remains unclear whether this summer peak represents the annual maximum.

In the Central USWC, dFe concentrations exhibit high variability but reach a maximum in February, several months prior to peak upwelling in the region (June; Figure S19). Similarly, in the Southern USWC, dFe concentrations peak in December, again several months earlier than the upwelling maxima, which occur first in April and then, more weakly, in August (Figure S19). Thus, the seasonality of dFe concentrations in the Central and Southern USWC, as revealed by our compilation, is unexpected and inconsistent with the anticipated dominant role of upwelling in regulating seasonal variability.

In the central USWC, Johnson et al. (2001) hypothesized that the peak in dFe concentrations in late winter/early spring results from the entrainment of Fe particle–rich waters from the benthic boundary layer, thereby increasing dissolvable Fe

https://doi.org/10.5194/egusphere-2026-4502
Preprint. Discussion started: 4 August 2026

concentrations. As upwelling begins and isopycnal surfaces tilt, water reaching the surface may spend less time in contact with the boundary layer on the inner shelf, resulting in little resuspended (dissolvable) Fe reaching the surface.

Building on this picture, Elrod et al. (2008) showed that a benthic boundary layer enriched in fine-grained, easily suspended sediment accumulates Fe-rich particles during river discharge associated with winter storm events. This layer is resuspended by strong winds during the first upwelling event and transported to the surface. It is then depleted, and subsequent upwelling events carry fewer Fe-rich particles to the surface. This conceptual framework is consistent with the seasonal shelf Fe reservoir proposed by Siedlecki et al. (2012), in which winter river discharge and sediment accumulation replenish a benthic reservoir of particulate Fe that is progressively tapped during the upwelling season, linking terrestrial inputs, sediment resuspension, and seasonal Fe supply to the California Current.

In the Southern USWC, the synchronicity between the seasonal cycle of surface dFe and those of major macronutrients may reflect the transport of low-dFe subsurface waters during upwelling or the influence of other processes, such as wintertime mixing, which has been shown to affect the seasonal variability of nitrate in the Southern USWC Damien et al. (2023b). In addition, seasonal dust deposition events (September to May) may supply substantial amounts of Fe to the region Deutsch et al. (2021), potentially playing a more significant role than upwelling or mixing in controlling seasonal variability. Whatever the underlying cause, this asynchronicity may also reflect limitations in the available data. Long-term time-series measurements of Fe, such as those from the Bermuda Atlantic Time-series Study (BATS) Sedwick et al. (2023) and Hawaii Ocean Time-series (HOT) at station ALOHA Bates and Hawco (2025), are needed to better characterize the seasonal variability of dFe along the USWC and to disentangle the processes driving it Tagliabue et al. (2023); Sofen et al. (2023).

In summary, our compilation provides the first comprehensive synthesis of Fe and ligand measurements along the USWC and offers new insights into the processes controlling the Fe cycle in a complex continental margin system. By integrating diverse datasets, it enables broader tests of hypotheses regarding Fe sources, transformations, and controls—an essential step toward constraining regional and global Fe budgets and models. Continued efforts to expand and harmonize measurements, particularly in under-sampled regions and seasons (e.g., winter in the Northern USWC), and to characterize different Fe species, are critical for advancing this understanding. Broad observational syntheses such as this are increasingly important for improving biogeochemical and Earth system models, especially as existing datasets remain dominated by open-ocean observations, whereas margin processes exert a disproportionate influence on the oceanic Fe cycle.

Acknowledgements. Funding for this work was provided by the US National Science Foundation, grant OCE-2343357 to AP and grants OCE-2023493 and OCE-1847687 to DB. This work used the Expanse system at the San Diego Supercomputer Center through allocation TG-OCE170017 from the Advanced Cyber infrastructure Coordination Ecosystem: Services and Support (ACCESS) program, which is supported by National Science Foundation grants 2138259, 2138286, 2138307, 2137603, and 2138296. Dissolved iron measurements from Till et al (in prep) funded by the Research Corporation for Science Advancement's Cottrell Scholar Award 26844 to CT.

Code and data availability.

https://doi.org/10.5194/egusphere-2026-4502
Preprint. Discussion started: 4 August 2026

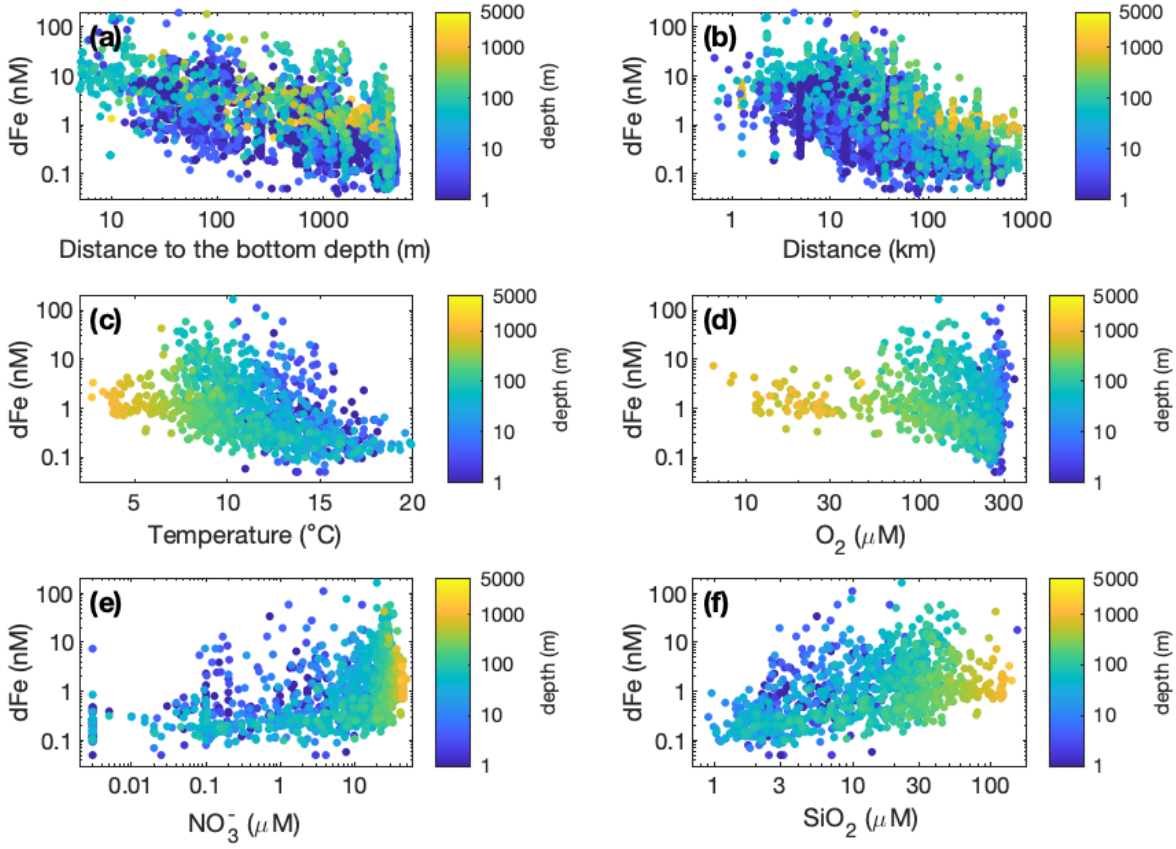

Figure 9. Relationship between dFe concentrations (nM) and co-located environmental variables along the US West Coast. Co-location was performed by mapping all variables onto a three-dimensional grid with a horizontal resolution of 0.25°and 32 unevenly spaced vertical levels (see Figure 1), at monthly climatological resolution, irrespective of the year of the measurements. Colors show depth (m).

MATLAB Code to reproduce figures can be found can be found on the Zenodo repository, under the following DOI: doi.org/10.5281/zenodo.11068852.

Data availability.

The compilation of Fe observations can be found on the Zenodo repository, under the following DOI: doi.org/10.5281/zenodo.11068852.

Author contributions.

https://doi.org/10.5194/egusphere-2026-4502
Preprint. Discussion started: 4 August 2026

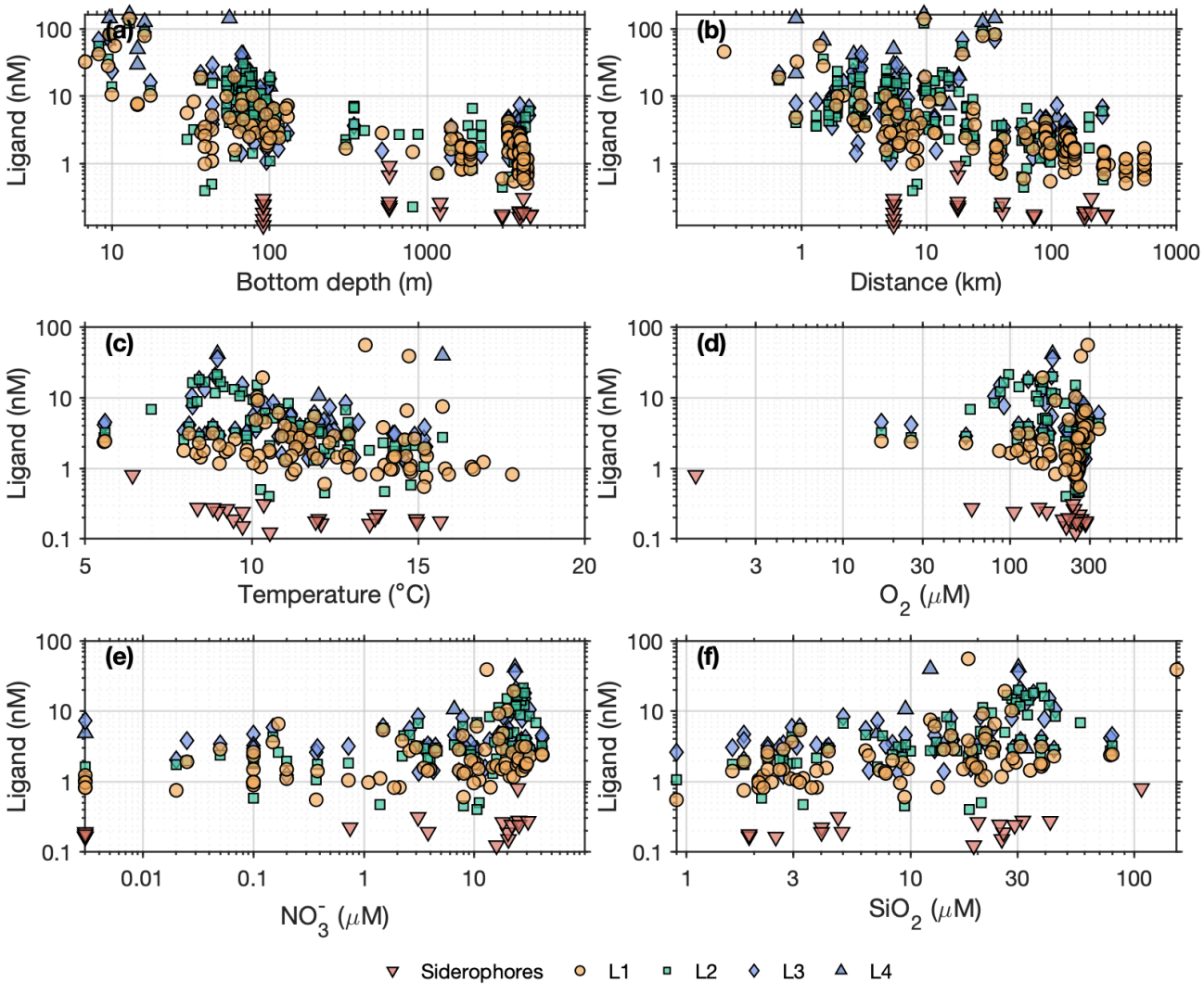

Figure 10. Relationship between ligand concentrations (nM) and co-located environmental variables along the US West Coast. Co-location was performed by mapping all variables onto a three-dimensional grid with a horizontal resolution of 0.25° and 32 unevenly spaced vertical levels (see Figure 1), at monthly climatological resolution, irrespective of the year of the measurements. Colors show depth (m). Different colored symbols represent different types of ligands (Siderophores, L1, L2, L3, and L4 - see the legend and section 2).

https://doi.org/10.5194/egusphere-2026-4502
Preprint. Discussion started: 4 August 2026

Competing interests.

The authors declare that they have no competing interests.

https://doi.org/10.5194/egusphere-2026-4502
Preprint. Discussion started: 4 August 2026

References

Bates, E. S. and Hawco, N. J.: Dissolved Iron Seasonal Cycle and Residence Time in the North Pacific Subtropical Gyre, Geophysical Research Letters, 52, e2025GL118 095, https://doi.org/https://doi.org/10.1029/2025GL118095, e2025GL118095 2025GL118095, 2025.

Biller, D. V. and Bruland, K. W.: Sources and distributions of Mn, Fe, Co, Ni, Cu, Zn, and Cd relative to macronutrients along the central California coast during the spring and summer upwelling season, Marine Chemistry, 155, 50–70, https://doi.org/https://doi.org/10.1016/j.marchem.2013.06.003, 2013.

Bograd, S. J., Schroeder, I. D., and Jacox, M. G.: A water mass history of the Southern California current system, Geophysical Research Letters, 46, 6690–6698, https://doi.org/https://doi.org/10.1029/2019GL082685, 2019.

Boiteau, R. M., Till, C. P., Coale, T. H., Fitzsimmons, J. N., Bruland, K. W., and Repeta, D. J.: Patterns of iron and siderophore distributions across the California Current System, Limnology and Oceanography, 64, 376–389, https://doi.org/https://doi.org/10.1002/lno.11046, 2019.

Bruland, K. and Lohan, M.: 6.02 - Controls of Trace Metals in Seawater, in: Treatise on Geochemistry, edited by Holland, H. D. and Turekian, K. K., pp. 23–47, Pergamon, Oxford, ISBN 978-0-08-043751-4, https://doi.org/https://doi.org/10.1016/B0-08-043751-6/06105-3, 2003.

Buck, K. N., Lohan, M. C., Berger, C. J. M., and Bruland, K. W.: Dissolved iron speciation in two distinct river plumes and an estuary: Implications for riverine iron supply, Limnology and Oceanography, 52, 843–855, https://doi.org/https://doi.org/10.4319/lo.2007.52.2.0843, 2007.

Buck, K. N., Selph, K. E., and Barbeau, K. A.: Iron-binding ligand production and copper speciation in an incubation experiment of Antarctic Peninsula shelf waters from the Bransfield Strait, Southern Ocean, Marine Chemistry, 122, 148–159, https://doi.org/http://dx.doi.org/10.1016/j.marchem.2010.06.002, 2010.

Bundy, R. M., Biller, D. V., Buck, K. N., Bruland, K. W., and Barbeau, K. A.: Distinct pools of dissolved iron-binding ligands in the surface and benthic boundary layer of the California Current, Limnology and Oceanography, 59, 769–787, https://doi.org/https://doi.org/10.4319/lo.2014.59.3.0769, 2014.

Bundy, R. M., Abdulla, H. A., Hatcher, P. G., Biller, D. V., Buck, K. N., and Barbeau, K. A.: Iron-binding ligands and humic substances in the San Francisco Bay estuary and estuarine-influenced shelf regions of coastal California, Marine Chemistry, 173, 183–194, https://doi.org/https://doi.org/10.1016/j.marchem.2014.11.005, sCOR WG 139: Organic Ligands – A Key Control on Trace Metal Biogeochemistry in the Ocean, 2015.

Bundy, R. M., Jiang, M., Carter, M., and Barbeau, K. A.: Iron-Binding Ligands in the Southern California Current System: Mechanistic Studies, Frontiers in Marine Science, 3, https://doi.org/10.3389/fmars.2016.00027, 2016.

Chase, Z., Johnson, K. S., Elrod, V. A., Plant, J. N., Fitzwater, S. E., Pickell, L., and Sakamoto, C. M.: Manganese and iron distributions off central California influenced by upwelling and shelf width, Marine Chemistry, 95, 235–254, https://doi.org/https://doi.org/10.1016/j.marchem.2004.09.006, 2005.

Chase, Z., Strutton, P. G., and Hales, B.: Iron links river runoff and shelf width to phytoplankton biomass along the U.S. West Coast, Geophysical Research Letters, 34, https://doi.org/https://doi.org/10.1029/2006GL028069, 2007.

Checkley, D. M. and Barth, J. A.: Patterns and processes in the California Current System, Progress in Oceanography, 83, 49–64, https://doi.org/https://doi.org/10.1016/j.pocean.2009.07.028, eastern Boundary Upwelling Ecosystems: Integrative and Comparative Approaches, 2009.

Conway, T. M. and John, S. G.: Quantification of dissolved iron sources to the North Atlantic Ocean, Nature, 511, 212–215, 2014.

https://doi.org/10.5194/egusphere-2026-4502
Preprint. Discussion started: 4 August 2026

Dale, A. W., Nickelsen, L., Scholz, F., Hensen, C., Oschlies, A., and Wallmann, K.: A revised global estimate of dissolved iron fluxes from marine sediments, Global Biogeochemical Cycles, 29, 691–707, 2015.

Damien, P., Bianchi, D., Kessouri, F., and McWilliams, J. C.: Modulation of Phytoplankton Uptake by Mesoscale and Submesoscale Eddies in the California Current System, Geophysical Research Letters, 50, e2023GL104 853, https://doi.org/https://doi.org/10.1029/2023GL104853, e2023GL104853 2023GL104853, 2023a.

Damien, P., Bianchi, D., McWilliams, J. C., Kessouri, F., Deutsch, C., Chen, R., and Renault, L.: Enhanced Biogeochemical Cycling Along the U.S. West Coast Shelf, Global Biogeochemical Cycles, 37, e2022GB007 572, https://doi.org/https://doi.org/10.1029/2022GB007572, e2022GB007572 2022GB007572, 2023b.

Deutsch, C., Frenzel, H., McWilliams, J. C., Renault, L., Kessouri, F., Howard, E., Liang, J.-H., Bianchi, D., and Yang, S.: Biogeochemical variability in the California Current System, Progress in Oceanography, 196, 102 565, https://doi.org/https://doi.org/10.1016/j.pocean.2021.102565, 2021.

Elrod, V. A., Berelson, W. M., Coale, K. H., and Johnson, K. S.: The flux of iron from continental shelf sediments: A missing source for global budgets, Geophysical Research Letters, 31, L12 307, https://doi.org/10.1029/2004GL020216, 2004.

Elrod, V. A., Johnson, K. S., Fitzwater, S. E., and Plant, J. N.: A long-term, high-resolution record of surface water iron concentrations in the upwelling-driven central California region, Journal of Geophysical Research: Oceans, 113, https://doi.org/https://doi.org/10.1029/2007JC004610, 2008.

Evans, N., Schroeder, I. D., Pozo Buil, M., Jacox, M. G., and Bograd, S. J.: Drivers of Subsurface Deoxygenation in the Southern California Current System, Geophysical Research Letters, 47, e2020GL089 274, https://doi.org/https://doi.org/10.1029/2020GL089274, e2020GL089274 2020GL089274, 2020.

Evans, N., Floback, A. E., Gaffney, J., Chace, P. J., Luna, Z., Knoery, J., Reimers, C. E., and Moffett, J. W.: The role of seasonal hypoxia and benthic boundary layer exchange on iron redox cycling on the Oregon shelf, Limnology and Oceanography, 69, 742–756, https://doi.org/https://doi.org/10.1002/lno.12476, 2024.

Fiechter, J. and Moore, A. M.: Iron limitation impact on eddy-induced ecosystem variability in the coastal Gulf of Alaska, Journal of Marine Systems, 92, 1–15, https://doi.org/https://doi.org/10.1016/j.jmarsys.2011.09.012, 2012.

Fitzwater, S. E., Johnson, K. S., Elrod, V. A., Ryan, J. P., Coletti, L. J., Tanner, S. J., Gordon, R., and Chavez, F. P.: Iron, nutrient and phytoplankton biomass relationships in upwelled waters of the California coastal system, Continental Shelf Research, 23, 1523–1544, https://doi.org/https://doi.org/10.1016/j.csr.2003.08.004, 2003.

Floback, A. E., Pham, A. L.-D., Damien, P., Odendahl, C. E., Weiske, J., Thomas, K. E., Gaffney, J., John, S. G., Bianchi, D., and Moffett, J. W.: Iron supply from the Oregon margin to the ocean dominated by hypoxia-dependent particles, Proceedings of the National Academy of Sciences, 123, e2532929 123, https://doi.org/10.1073/pnas.2532929123, 2026.

Forsch, K. O., Fulton, K. C., Weiss, M. M., Krause, J. W., Stukel, M. R., and Barbeau, K. A.: Iron Limitation and Biogeochemical Effects in Southern California Current Coastal Upwelling Filaments, Journal of Geophysical Research: Oceans, 128, e2023JC019 961, https://doi.org/https://doi.org/10.1029/2023JC019961, e2023JC019961 2023JC019961, 2023.

Gangrade, S., Franks, P. J. S., Forsch, K. O., and Barbeau, K. A.: Salinity is diagnostic of maximum potential chlorophyll and phytoplankton community structure in an Eastern Boundary Upwelling System, Limnology and Oceanography Letters, 10, 923–933, https://doi.org/https://doi.org/10.1002/lol2.70059, 2025.

Gledhill, M. and Buck, K.: The Organic Complexation of Iron in the Marine Environment: A Review, Frontiers in Microbiology, 3, https://doi.org/10.3389/fmicb.2012.00069, 2012.

https://doi.org/10.5194/egusphere-2026-4502
Preprint. Discussion started: 4 August 2026

Hassler, C. S., Simó, R., Fawcett, S. E., Ellwood, M. J., and Jaccard, S. L.: Marine biogenic humic substances control iron biogeochemistry across the Southern Ocean, Nature Communications, 16, 2662, https://doi.org/10.1038/s41467-025-57491-5, 2025.

Hogle, S. L., Dupont, C. L., Hopkinson, B. M., King, A. L., Buck, K. N., Roe, K. L., Stuart, R. K., Allen, A. E., Mann, E. L., Johnson, Z. I., and Barbeau, K. A.: Pervasive iron limitation at subsurface chlorophyll maxima of the California Current, Proceedings of the National Academy of Sciences, 115, 13 300–13 305, https://doi.org/10.1073/pnas.1813192115, 2018.

Homoky, W. B., Conway, T. M., John, S. G., König, D., Deng, F., Tagliabue, A., and Mills, R. A.: Iron colloids dominate sedimentary supply to the ocean interior, Proceedings of the National Academy of Sciences, 118, e2016078 118, https://doi.org/10.1073/pnas.2016078118, 2021.

Jacox, M. G., Edwards, C. A., Hazen, E. L., and Bograd, S. J.: Coastal Upwelling Revisited: Ekman, Bakun, and Improved Upwelling Indices for the U.S. West Coast, Journal of Geophysical Research: Oceans, 123, 7332–7350, https://doi.org/https://doi.org/10.1029/2018JC014187, 2018a.

Jacox, M. G., Edwards, C. A., Hazen, E. L., and Bograd, S. J.: Coastal upwelling revisited: Ekman, Bakun, and improved upwelling indices for the US West Coast, Journal of Geophysical Research: Oceans, 123, 7332–7350, 2018b.

Johnson, K. S., Chavez, F. P., and Friederich, G. E.: Continental-shelf sediment as a primary source of iron for coastal phytoplankton, Nature, 398, 697–700, http://dx.doi.org/10.1038/19511, 1999.

Johnson, K. S., Chavez, F. P., Elrod, V. A., Fitzwater, S. E., Pennington, J. T., Buck, K. R., and Walz, P. M.: The annual cycle of iron and the biological response in central California coastal waters, Geophysical Research Letters, 28, 1247–1250, https://doi.org/https://doi.org/10.1029/2000GL012433, 2001.

Johnson, K. S., Elrod, V. A., Fitzwater, S. E., Plant, J. N., Chavez, F. P., Tanner, S. J., Gordon, R. M., Westphal, D. L., Perry, K. D., Wu, J., and Karl, D. M.: Surface ocean-lower atmosphere interactions in the Northeast Pacific Ocean Gyre: Aerosols, iron, and the ecosystem response, Global Biogeochemical Cycles, 17, https://doi.org/https://doi.org/10.1029/2002GB002004, 2003.

King, A. L. and Barbeau, K. A.: Dissolved iron and macronutrient distributions in the southern California Current System, Journal of Geophysical Research: Oceans, 116, https://doi.org/https://doi.org/10.1029/2010JC006324, 2011.

King, A. L., Buck, K. N., and Barbeau, K. A.: Quasi-Lagrangian drifter studies of iron speciation and cycling off Point Conception, California, Marine Chemistry, 128-129, 1–12, https://doi.org/https://doi.org/10.1016/j.marchem.2011.11.001, 2012.

Krachler, R. and Krachler, R. F.: Northern High-Latitude Organic Soils As a Vital Source of River-Borne Dissolved Iron to the Ocean, Environmental Science & Technology, 55, 9672–9690, https://doi.org/10.1021/acs.est.1c01439, 2021.

Lam, P. J. and Bishop, J. K. B.: The continental margin is a key source of iron to the HNLC North Pacific Ocean, Geophysical Research Letters, 35, https://doi.org/https://doi.org/10.1029/2008GL033294, 2008.

Lam, P. J., Heller, M. I., Lerner, P. E., Moffett, J. W., and Buck, K. N.: Unexpected Source and Transport of Iron from the Deep Peru Margin, ACS Earth and Space Chemistry, 4, 977–992, https://doi.org/10.1021/acsearthspacechem.0c00066, 2020.

Li, J., Babcock-Adams, L., Boiteau, R. M., McIlvin, M. R., Manck, L. E., Sieber, M., Lanning, N. T., Bundy, R. M., Bian, X., Ștreangă, I.-M., Granzow, B. N., Church, M. J., Fitzsimmons, J. N., John, S. G., Conway, T. M., and Repeta, D. J.: Microbial iron limitation in the ocean's twilight zone, Nature, 633, 823–827, https://doi.org/10.1038/s41586-024-07905-z, 2024.

Lynn, R. J. and Simpson, J. J.: The California Current system: The seasonal variability of its physical characteristics, Journal of Geophysical Research: Oceans, 92, 12 947–12 966, https://doi.org/https://doi.org/10.1029/JC092iC12p12947, 1987.

McClatchie, S.: Regional fisheries oceanography of the California Current System, Springer, Springer Dordrecht Heidelberg New York London, ISBN 978-94-007-7222-9, https://doi.org/10.1007/978-94-007-7223-6, 2016.

https://doi.org/10.5194/egusphere-2026-4502
Preprint. Discussion started: 4 August 2026

Moffett, J. W. and Boiteau, R. M.: Metal Organic Complexation in Seawater: Historical Background and Future Directions, Annual Review of Marine Science, 16, null, https://doi.org/10.1146/annurev-marine-033023-083652, pMID: 37722713, 2024.

Olsen, A., Lange, N., Key, R. M., Tanhua, T., Álvarez, M., Becker, S., Bittig, H. C., Carter, B. R., Cotrim da Cunha, L., Feely, R. A., van Heuven, S., Hoppema, M., Ishii, M., Jeansson, E., Jones, S. D., Jutterström, S., Karlsen, M. K., Kozyr, A., Lauvset, S. K., Lo Monaco, C., Murata, A., Pérez, F. F., Pfeil, B., Schirnick, C., Steinfeldt, R., Suzuki, T., Telszewski, M., Tilbrook, B., Velo, A., and Wanninkhof, R.: GLODAPv2.2019 – an update of GLODAPv2, Earth System Science Data, 11, 1437–1461, https://doi.org/10.5194/essd-11-1437-2019, 2019.

Pham, A. L. D. and Ito, T.: Formation and Maintenance of the GEOTRACES Subsurface-Dissolved Iron Maxima in an Ocean Biogeochemistry Model, Global Biogeochemical Cycles, 32, 932–953, https://doi.org/10.1029/2017GB005852, 2018.

Pham, A. L.-D., Damien, P., McCoy, D., Mar, M., Kessouri, F., McWilliams, J. C., Moffett, J., and Bianchi, D.: The Shelf-To-Basin Transport of Iron From the Northern U.S. West Coast to the Pacific Ocean, Global Biogeochemical Cycles, 38, e2023GB008 029, https://doi.org/https://doi.org/10.1029/2023GB008029, e2023GB008029 2023GB008029, 2024.

Robinson, D., Pham, A. L., Yousavich, D. J., Janssen, F., Wenzhöfer, F., Arrington, E. C., Gosselin, K. M., Sandoval-Belmar, M., Mar, M., Valentine, D. L., et al.: Iron "Ore" Nothing: Benthic iron fluxes from the oxygen-deficient Santa Barbara Basin enhance phytoplankton productivity in surface waters, Biogeosciences Discussions, pp. 1–36, 2022.

Rue, E. L. and Bruland, K. W.: Complexation of iron(III) by natural organic ligands in the Central North Pacific as determined by a new competitive ligand equilibration/adsorptive cathodic stripping voltammetric method, Marine Chemistry, 50, 117–138, https://doi.org/http://dx.doi.org/10.1016/0304-4203(95)00031-L, 1995.

Sandoval-Belmar, M., Smith, J., Moreno, A. R., Anderson, C., Kudela, R. M., Sutula, M., Kessouri, F., Caron, D. A., Chavez, F. P., and Bianchi, D.: A cross-regional examination of patterns and environmental drivers of Pseudo-nitzschia harmful algal blooms along the California coast, Harmful Algae, 126, 102 435, https://doi.org/https://doi.org/10.1016/j.hal.2023.102435, 2023.

Sedwick, P. N., Sohst, B. M., Buck, K. N., Caprara, S., Johnson, R. J., Ohnemus, D. C., Sofen, L. E., Tagliabue, A., Twining, B. S., and Williams, T. E.: Atmospheric Input and Seasonal Inventory of Dissolved Iron in the Sargasso Sea: Implications for Iron Dynamics in Surface Waters of the Subtropical Ocean, Geophysical Research Letters, 50, e2022GL102 594, https://doi.org/https://doi.org/10.1029/2022GL102594, e2022GL102594 2022GL102594, 2023.

Severmann, S., McManus, J., Berelson, W. M., and Hammond, D. E.: The continental shelf benthic iron flux and its isotope composition, Geochimica et Cosmochimica Acta, 74, 3984–4004, https://doi.org/http://dx.doi.org/10.1016/j.gca.2010.04.022, 2010.

Siedlecki, S. A., Mahadevan, A., and Archer, D. E.: Mechanism for export of sediment-derived iron in an upwelling regime, Geophysical Research Letters, 39, https://doi.org/https://doi.org/10.1029/2011GL050366, 2012.

Sofen, L. E., Antipova, O. A., Buck, K. N., Caprara, S., Chacho, L., Johnson, R. J., Kim, G., Morton, P., Ohnemus, D. C., Rauschenberg, S., Sedwick, P. N., Tagliabue, A., and Twining, B. S.: Authigenic Iron Is a Significant Component of Oceanic Labile Particulate Iron Inventories, Global Biogeochemical Cycles, 37, e2023GB007 837, https://doi.org/https://doi.org/10.1029/2023GB007837, e2023GB007837 2023GB007837, 2023.

Tagliabue, A., Mtshali, T., Aumont, O., Bowie, A. R., Klunder, M. B., Roychoudhury, A. N., and Swart, S.: A global compilation of dissolved iron measurements: focus on distributions and processes in the Southern Ocean, Biogeosciences, 9, 2333–2349, https://doi.org/10.5194/bg-9-2333-2012, 2012.

https://doi.org/10.5194/egusphere-2026-4502
Preprint. Discussion started: 4 August 2026

Tagliabue, A., Sallee, J.-B., Bowie, A. R., Levy, M., Swart, S., and Boyd, P. W.: Surface-water iron supplies in the Southern Ocean sustained by deep winter mixing, Nature Geosci, 7, 314–320, https://doi.org/10.1038/ngeo2101 http://www.nature.com/ngeo/journal/v7/n4/abs/ngeo2101.html#supplementary-information, 2014.

Tagliabue, A., Bowie, A. R., Boyd, P. W., Buck, K. N., Johnson, K. S., and Saito, M. A.: The integral role of iron in ocean biogeochemistry, Nature, 543, 51–59, https://doi.org/10.1038/nature21058, 2017.

Tagliabue, A., Buck, K. N., Sofen, L. E., Twining, B. S., Aumont, O., Boyd, P. W., Caprara, S., Homoky, W. B., Johnson, R., König, D., Ohnemus, D. C., Sohst, B., and Sedwick, P.: Authigenic mineral phases as a driver of the upper-ocean iron cycle, Nature, 620, 104–109, https://doi.org/10.1038/s41586-023-06210-5, 2023.

Till, C. P., Solomon, J. R., Cohen, N. R., Lampe, R. H., Marchetti, A., Coale, T. H., and Bruland, K. W.: The iron limitation mosaic in the California Current System: Factors governing Fe availability in the shelf/near-shelf region, Limnology and Oceanography, 64, 109–123, https://doi.org/https://doi.org/10.1002/lno.11022, 2019.

Tortell, P. D., Maldonado, M. T., and Price, N. M.: The role of heterotrophic bacteria in iron-limited ocean ecosystems, Nature, 383, 330–332, https://doi.org/10.1038/383330a0, 1996.

Vieira, L. H., Krisch, S., Hopwood, M. J., Beck, A. J., Scholten, J., Liebetrau, V., and Achterberg, E. P.: Unprecedented Fe delivery from the Congo River margin to the South Atlantic Gyre, Nature Communications, 11, 556, https://doi.org/10.1038/s41467-019-14255-2, 2020.

Völker, C. and Tagliabue, A.: Modeling organic iron-binding ligands in a three-dimensional biogeochemical ocean model, Marine Chemistry, 173, 67–77, https://doi.org/http://dx.doi.org/10.1016/j.marchem.2014.11.008, 2015.

Wetz, M. S., Hales, B., Chase, Z., Wheeler, P. A., and Whitney, M. M.: Riverine input of macronutrients, iron, and organic matter to the coastal ocean off Oregon, U.S.A., during the winter, Limnology and Oceanography, 51, 2221–2231, https://doi.org/https://doi.org/10.4319/lo.2006.51.5.2221, 2006.

Wong, K. H., Nishioka, J., Kim, T., and Obata, H.: Long-Range Lateral Transport of Dissolved Manganese and Iron in the Subarctic Pacific, Journal of Geophysical Research: Oceans, 127, e2021JC017 652, https://doi.org/https://doi.org/10.1029/2021JC017652, e2021JC017652 2021JC017652, 2022.

Zaba, K. D., Franks, P. J. S., and Ohman, M. D.: The California Undercurrent as a Source of Upwelled Waters in a Coastal Filament, Journal of Geophysical Research: Oceans, 126, e2020JC016 602, https://doi.org/https://doi.org/10.1029/2020JC016602, e2020JC016602 2020JC016602, 2021.